Article

When is a Nanoparticle a Cluster? An Operando EXAFS Study of Amine Borane Dehydrocoupling by Rh Clusters

John L. Fulton, John C. Linehan, Tom Autrey, Mahalingam Balasubramanian, Yongsheng Chen, and Nathaniel K. Szymczak

J. Am. Chem. Soc., **2007**, 129 (39), 11936-11949• DOI: 10.1021/ja073331l • Publication Date (Web): 07 September 2007

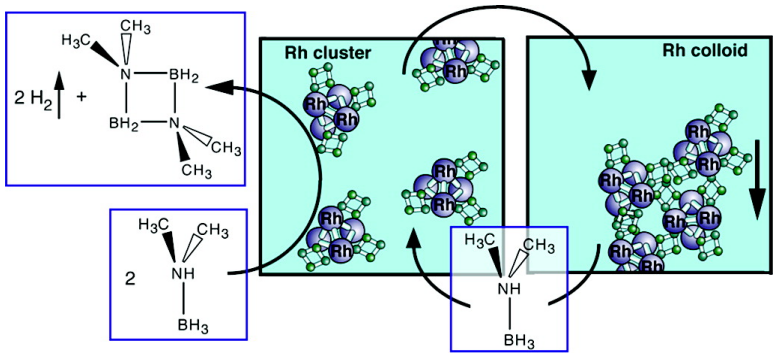

More About This Article

Additional resources and features associated with this article are available within the HTML version:

- Supporting Information
- Links to the 10 articles that cite this article, as of the time of this article download
- Access to high resolution figures
- Links to articles and content related to this article
- Copyright permission to reproduce figures and/or text from this article

View the Full Text HTML

J|A|C|S
ARTICLES
Published on Web 09/07/2007

When is a Nanoparticle a Cluster? An Operando EXAFS Study of Amine Borane Dehydrocoupling by Rh_{4-6} Clusters

John L. Fulton,*,† John C. Linehan,*,† Tom Autrey,† Mahalingam Balasubramanian,‡ Yongsheng Chen,† and Nathaniel K. Szymczak§

Contribution from the Fundamental Science Directorate, Pacific Northwest National Laboratory, Richland, Washington, 99352, Advanced Photon Source, Argonne National Laboratory, Argonne, Illinois 60439, and Chemistry Department, University of Oregon, Eugene, Oregon 97403

Received May 10, 2007; E-mail: john.linehan@pnl.gov; john.fulton@pnl.gov

Abstract: X-ray absorption fine structure (XAFS) is used to determine the structure of the rhodium cluster present during the catalyzed dehydrocoupling of amine boranes under *operando* conditions. We show how a variety of XAFS strategies can be used in combination with other analytical methods to differentiate homogeneous from heterogeneous systems. Analysis of the *in situ* XAFS spectra using a series of amine boranes (NH_3BH_3, R_2NHBH_3, and RNH_2BH_3 where R = methyl, isopropyl, *tert*-butyl, and cyclohexyl) and rhodium catalyst precursor compounds (including chloro-(1,5-cyclooctadiene)rhodium (I) dimer, bis(1,5-cyclooctadiene)rhodium (I) trifluoromethanesulfonate, chlorodicarbonylrhodium (I) dimer, dichloro(pentamethylcylcopentadienyl)rhodium (III) dimer, hexarhodium hexadecacarbonyl, and tetrarhodium dodecacarbonyl) strongly suggest that the active catalyst species for this reaction is a homogeneous rhodium complex. Rhodium clusters containing four or six rhodium atoms (Rh_{4-6}) bound to amine boranes are observed as the major (>99%) rhodium containing species during and after the catalyzed anaerobic dehydrocoupling. During the later stages of the reaction a nonmetallic rhodium complex precipitates in which individual Rh_{4-6} clusters likely form polymer chains ligated by the reaction products that have two or more ligating sites. The best fits of the XAFS data, using ab initio calculations of FEFF theory, show that the major rhodium species (80%) has each rhodium atom directly bound to three rhodium atoms with an observed bond distance of 2.73 Å and to two boron atoms at 2.10 Å. A minor (20%) rhodium species has each rhodium atom bound to four rhodium atoms with a bond distance of about 2.73 Å and a single rhodium atom at a nonbonding distance of 3.88 Å. No metallic rhodium was observed at any time during the anaerobic reaction.

1. Introduction

Hydrogen-rich amine borane compounds such as NH_3BH_3 (AB) are considered potential materials for hydrogen storage for fuel cell applications which has stimulated recent interest in understanding their chemistry.[1−10] The bonding of hydrogen to the light atoms, nitrogen and boron, can meet the required energy density goals for hydrogen storage. Rhodium-based catalysts are known to efficiently catalyze dehydrocoupling of amine boranes under ambient conditions to release H_2 with formation of borazines, and boron-nitrogen oligomers. In addition, we have shown that there is an enhanced release of H_2 during the thermal dehydrocoupling of NH_3BH_3 at the surface of mesoporous silica.[11] This rhodium-catalyzed amine borane chemistry has been the subject of several comprehensive studies by Manners et al.[12,13] Our initial *in situ* work[14] in this area suggested that small Rh_n clusters (n = 4−6) are the catalytically active species for the dehydrocoupling of $(CH_3)_2$-$NHBH_3$ (DMAB) as shown in eq 1 although *ex situ* characterization suggested a much larger colloidal metallic rhodium species.[13] The goal of this work is to develop a detailed understanding of the role of the rhodium-containing catalyst in the dehydrocoupling of amine borane compounds.

It has become clear in recent years that the *ex situ* characterization of colloidal or nanoparticle catalyst species can be

† Pacific Northwest National Laboratory.
‡ Argonne National Laboratory.
§ University of Oregon.

(1) Baitalow, F.; Wolf, G.; Grolier, J. P. E.; Dan, F.; Randzio, S. L. *Thermochim. Acta* **2006**, *445*, 121.
(2) Baumann, J.; Baitalow, E.; Wolf, G. *Thermochim. Acta* **2005**, *430*, 9.
(3) Bluhm, M. E.; Bradley, M. G.; Butterick, R.; Kusari, U.; Sneddon, L. G. *J. Am. Chem. Soc.* **2006**, *128*, 7748.
(4) Dixon, D. A.; Gutowski, M. *J. Phys. Chem.* A **2005**, *109*, 5129.
(5) Grant, D. J.; Dixon, D. A. *J. Phys. Chem.* A **2005**, *109*, 10138.
(6) Keaton, R. J.; Blacquiere, J. M.; Baker, R. T. *J. Am. Chem. Soc.* **2007**, *129*, 1844.
(7) Matus, M. H.; Nguyen, M. T.; Dixon, D. A. *J. Phys. Chem. A* **2007**, *111*, 1726.
(8) Nguyen, M. T.; Nguyen, V. S.; Matus, M. H.; Gopakumar, G.; Dixon, D. A. *J. Phys. Chem. A* **2007**, *111*, 679.
(9) Stephens, F. H.; Baker, R. T.; Matus, M. H.; Grant, D. J.; Dixon, D. A. *Angew. Chem., Int. Ed.* **2007**, *46*, 746.
(10) Yoon, C. W.; Sneddon, L. G. *J. Am. Chem. Soc.* **2006**, *128*, 13992.
(11) Gutowska, A.; Li, L. Y.; Shin, Y. S.; Wang, C. M. M.; Li, X. H. S.; Linehan, J. C.; Smith, R. S.; Kay, B. D.; Schmid, B.; Shaw, W.; Gutowski, M.; Autrey, T. *Angew. Chem., Int. Ed.* **2005**, *44*, 3578.
(12) Jaska, C. A.; Temple, K.; Lough, A. J.; Manners, I. *J. Am. Chem. Soc.* **2003**, *125*, 9424.
(13) Jaska, C. A.; Manners, I. *J. Am. Chem. Soc.* **2004**, *126*, 9776.
(14) Chen, Y. S.; Fulton, J. L.; Linehan, J. C.; Autrey, T. *J. Am. Chem. Soc.* **2005**, *127*, 3254.

10.1021/ja073331l CCC: $37.00

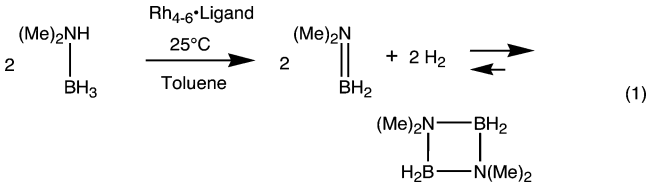

(1)

compromised by the measurement technique. For instance it has recently been shown[13,15] that, under commonly used TEM conditions, the electron beam can induce the formation of rhodium nanoparticles from rhodium organometallic complexes leading to ambiguous conclusions about the morphology of the active species. Adding to this challenging analysis problem is that the catalyst structure at the end of a reaction can be different than the structure during the reaction. For instance, the starting reactants or reaction intermediates may bind as ligands to the rhodium cluster, helping to stabilize the soluble form. As these initial reactants/ligands are consumed through the course of the reaction, their ability to stabilize the rhodium cluster in solution can be attenuated. It is therefore advantageous to use analytical spectroscopic methods that examine the form of the catalyst in the "*operando*" state, wherein the catalyst not only is in the reaction solvent, at the reaction pressure and temperature (i.e., *in situ*), but also is undergoing chemical reactions with the reactants in the system. *Operando* methods using NMR or FTIR are especially useful for following the reaction pathways and kinetics of the reactants, the products and with some limited capability for catalyst characterization. On the other hand, X-ray absorption fine structure (XAFS), employed as an *operando* method, can selectively probe the predominate metal species as the XAFS signal is primarily dependent on the backscattering from the first two or three atomic shells about the X-ray absorbing metal center. XAFS is also very useful for characterizing clusters in which the highly fluxional nature of the ligands and/or the ligand exchange rates are so high as to make identification by NMR difficult or impossible since the time frame of the complete XAFS scattering process (a few femtoseconds) is much shorter than the time for any changes in the atom positions.

In our previous communication[14] we proposed that, near the end of the reaction shown in eq 1, the rhodium cluster binds ligands from the product of the reaction, forming a precipitate comprising large numbers of individual rhodium clusters to yield an insoluble resting state of the rhodium catalyst species. In this work we present further evidence supporting this hypothesis. A related observation has been reported by Toshima[16] for small rhodium and platinum/rhodium clusters in a polymer-stabilized colloidal dispersion. Their XAFS measurement showed a cluster size of 13 rhodium atoms that was inconsistent with a TEM analysis of 3.3 nm (~500 atoms). They proposed a model of a rhodium "microcluster" embedded in a much larger polymer matrix. In this work we present a related rhodium structure in which a Rh_{4-6} cluster forms its own polymer-like network from products that are generated during a catalytic reaction. The solid precipitate that forms at the end of the reaction can be regenerated to the soluble active Rh_{4-6} cluster by simply adding more of the amine borane reactant. This highlights an interesting feature of this reaction, the ability to recover the active rhodium catalyst with high efficiencies by self-precipitation and then regeneration of the active catalyst for a subsequent catalytic cycle. This concept of a recyclable homogeneous catalyst is similar to that reported for a tungsten hydrosilylation catalyst that forms an insoluble chlathrate species at the end of the reaction.[17]

The ability of XAFS to derive the molecular structure of metal clusters randomly dispersed in a solvent provides an alternative to conventional single-crystal X-ray diffraction (XRD) when the cluster cannot be recovered in its crystalline form. The Rh_{4-6} clusters in this study have eight or more ligand sites, and the reaction products can form bridges between rhodium clusters thus making it difficult or impossible to generate a crystalline form for XRD analysis. The disadvantage of XAFS is that the ability to resolve the atom positions and atom types is not as conclusive as full crystallographic techniques such as XRD. Specifically, first shell ligands are often well-resolved, but there is decreasing resolution for the second and higher shells. However, in the present case, the rhodium−rhodium backscattering functions will be significantly different than the backscattering functions for boron, nitrogen, and carbon, and hence rhodium nearest neighbors can be detected with high sensitivity. This means that accurate determination of rhodium cluster sizes is possible with XAFS. On the other hand the backscattering functions for boron and nitrogen are quite similar, and thus these atom types can only be discriminated for certain highly optimum structures. Within these limitations the full structure may not be resolved without *a priori* information of the nature of the ligands about the metal atom. This is a situation where the combination of the two *operando* methods, XAFS and NMR, provides a powerful method to identify active catalyst structures. Another tool in understanding the ligand structure about the rhodium core is to conduct XAFS studies of a series of related reactant and catalyst precursor compounds thereby eliminating or allowing the possibilities of certain ligands. It is this combination of methodologies that we employ here to understand the nature of the active catalyst for dehydrocoupling reactions of a series of amine borane compounds.

In this report, we use *operando* XAFS methods to show that the active catalytic species is most likely a Rh_{4-6} cluster (diameter of approximately 0.3 nm) rather than a 2 nm diameter rhodium nanoparticle.[12,13] We then use a combination of the other methodologies described above to derive the most probable ligand structure about the rhodium cluster. The reported structure of the predominate rhodium species provides key insights into the likely catalytic species and the mechanism of the formation of hydrogen from amine borane compounds. Further we use XAFS to determine the kinetics of formation for the new rhodium clusters (presumably related to the catalyst species) and show that the material that precipitates at the end of the reaction contains the same rhodium cluster with only slightly different amine borane ligands. We anticipate this class of Rh_{4-6} clusters may play an important role in both dehydrocoupling and hydrogenation reactions.

2. Experimental Section

2.1. Chemicals and Procedures. Dimethylamine borane (Callery), *tert*-butylamine borane (*t*BAB, Callery), ammonia borane (Aviabor), bis(1,5-cyclooctadiene)rhodium (I) trifluoromethanesulfonate (Strem), chloro-(1,5-cyclooctadiene)rhodium (I) dimer (Strem), chlorodicarbo-

(15) Hagen, C. M.; Vieille-Petit, L.; Laurenczy, G.; Suss-Fink, G.; Finke, R. G. *Organometallics* **2005**, *24*, 1819.
(16) Harada, M.; Asakura, K.; Toshima, N. *J. Phys. Chem.* **1994**, *98*, 2653.
(17) Dioumaev, V. K.; Bullock, R. M. *Nature* **2003**, *424*, 530.

nylrhodium (I) dimer (Strem), dichloro(pentamethylcylcopentadienyl)rhodium (III) dimer (Strem), hexarhodium hexadecacarbonyl (Strem), and tetrarhodium dodecacarbonyl (Strem) were used as received. Di-isopropylamine borane (DiPAB), cyclohexylamine borane (CAB), and dicyclohexylamine borane (DCAB) were synthesized by addition of the appropriate amine to an equimolar amount of a THF solution of BH_3−THF complex.[18] The purity of all amine boranes used in this study was greater than 99% as determined by ^{1}H and ^{11}B NMR. Toluene and THF (Aldrich) were distilled from sodium and degassed prior to use. All reactions were carried out under an inert atmosphere unless otherwise stated.

The concentration of the precatalyst was varied between 3.5 and 35 mM, and that of the substrate, between 0.02 and 2 M. In a typical procedure a solution of 20 mg of chloro-(1,5-cyclooctadiene)rhodium (I) dimer ([Rh(1,5-COD)Cl]$_2$) dissolved in 2 mL of toluene was added to a solution containing 200 mg of DMAB in 2 mL of toluene under an atmosphere of 4% H_2 in He. The mixed solution inside of a 1.5 cm diameter × 6 cm long sealed glass vial was taken from the glovebox and placed in the X-ray beam. A new vial was used for each reaction. Each vial was placed in a horizontal position to provide a 6 cm path length for the X-ray beam. The glass sidewall of each vial was pierced with a 1 mm diameter hole to allow for escape of the H_2. To prevent the ingress of air into the reaction vial the side hole was covered with a 1 cm^2 piece of Kapton film. The first XAFS spectrum was collected within 3 min of mixing.

2.2. XAFS Methods. The rhodium K-edge (23222 eV) XAFS spectra were collected in transmission mode on the bending magnet beamline (XOR/PNC, Sector 20) at the Advanced Photon Source, Argonne National Laboratory. The bending magnet beamline was chosen over the much higher flux insertion device line to minimize the potential for beam damage to the rhodium complexes. No evidence of beam damage was observed during exposure of the rhodium complexes to the X-rays. Energy calibration was accomplished using the edge energy of a Rh(0) foil (23222 eV). As a further measure, this rhodium foil was placed far beyond the sample with an additional transmission detector (I_2) providing internal energy calibration for each sample spectrum. We collected time series of X-ray absorption near edge (XANES) spectra while the active catalyst was forming to study their kinetics. Full extended X-ray absorption fine structure (EXAFS) spectra were collected when the kinetics were slow or the conversion was complete in order to capture the most molecular structural information on the rhodium catalyst. Series of XANES spectra were normalized to a common edge height.

We used standard methods for the analysis of EXAFS data[19] using portions of the UWXAFS program.[20] The EXAFS relationship is given by

$$\chi(k) = \sum_i \frac{F_i(k)\, S_0^2 N_i}{kR_i^2} e^{-2k^2\sigma_i^2} e^{-2R_i/\lambda(k)} \sin(2kR_i + \delta_i(k)) \qquad (2)$$

The EXAFS oscillations, $\chi(k)$, were extracted from the experimentally measured absorption coefficient using an automated background subtraction method (AUTOBK) developed by Newville et al.[21] The wavenumber of the ejected photoelectron is given by $k = \sqrt{2m_e(E - E_0)/\hbar^2}$ with E_0 being the absorption edge energy. In eq 2, $F_i(k)$, $\delta_i(k)$, and $\lambda(k)$ are the amplitude, phase, and mean-free-path factor, respectively, that are derived from theoretical standards calculated by FEFF8.[22] The S_0^2 term in the above equation is the core-hole or amplitude-reduction factor and is usually treated empirically. The fitted parameters include N_i, the coordination number of the shell for each type of neighboring atom, R_i, the shell distance, and σ_i^2, the Debye−Waller factor which represents the mean-square variation in R_i due to both static and thermal disorder. The fitting of the FEFF8 theoretical standards to the experimental data was accomplished using an analysis program (FEFFIT).[23] In addition to the structural parameters, a single nonstructural parameter, ΔE_0, is varied to correct for the simple estimate of E_0 made by FEFF8.

Various rhodium-containing standard compounds were used to establish the value of the core-hole factor, S_0^2, and to also better understand the sensitivity of the XAFS method to the detection of longer range rhodium atoms. In evaluating these compounds the $\chi(k)$ data were fit to the FEFF8 theoretical standard using the atom positions that were generated from the published crystallographic data for dichloro-(pentamethylcylcopentadienyl)rhodium (III) dimer,[24] bis(1,5-cyclooctadiene)rhodium (I) trifluoromethanesulfonate, chlorodicarbonylrhodium (I) dimer,[25] $Rh_4(CO)_{12}$,[26] $Rh_6(CO)_{16}$,[27] chloro(1,5-cyclooctadiene)-rhodium (I) dimer,[28] and for rhodium metal.[29] (Schematics of these structures are given in the insets of Figures 9 and 10.) The complete fits to these standards are provided in the Supporting Information. When evaluating the new rhodium cluster, we used a core-hole factor of $S_0^2 = 0.89$, i.e., the average from the five different solid standards. S_0^2 has an associated uncertainty of about 15%, and according to eq 2, we see that this results in an approximate 15% uncertainty in the reported coordination number.

The EXAFS $\chi(k)$ data were weighted by k^2 and windowed in the range $2.0 < k < 17.0$ Å^{-1} using a Hanning window with $dk = 1.0$ Å^{-1}. The fits were to both the real and imaginary parts of $\tilde{\chi}(R)$ in the region $0.8 < R < 5.0$ Å. The quality of fits was evaluated using the criteria defined in FEFFIT, the automated software for fitting the structural parameters.

The structure of several Rh_4 clusters have been characterized by single-crystal XRD.[26,30] One cluster of particular relevance for this study is $Rh_4(CO)_{12}$ since the Rh coordination number is very close to that measured for the rhodium catalyst in this study. $Rh_4(CO)_{12}$ has C_3 symmetry with three equivalent rhodium atoms each binding two terminal CO's and sharing two bridging CO's. The fourth apical rhodium binds to only three terminal CO's. The rhodium−rhodium bond distances are only slightly different with rhodium bonds to the apical rhodium of about 2.675 Å and slightly longer bonds between the three equivalent rhodium atoms of 2.725 Å.[26] The structure is highly fluxional in solution, which makes it difficult to characterize by NMR.[31] In the FEFF8 calculations used in this study, $Rh_4(CO)_{12}$ was used as the base structure and modified by substituting B and N atoms at the same terminal and bridging sites modified by realistic Rh−B and Rh−N distances. Even with this more accurate representation of the rhodium cluster much simpler FEFF8 structures generated from a single rhodium atom coordinated with various B, N, or Rh ligands gave nearly identical fit results showing the invariance of the fitted results with respect to the starting model.

In several instances principal component analysis was used to fully evaluate the reaction rate and to determine the number of chemical states of the Rh species. In some systems, where only a limited number

(18) Brown, H. C.; Zaidlewicz, M.; Dalvi, P. V.; Narasimhan, S.; Mukhopadhyay, A. *Organometallics* **1999**, *18*, 1305.
(19) Koningsberger, D. C.; Prins, R. *X-ray Absorption: Principles, Applications, Techniques of EXAFS, SEXAFS and XANES*; John Wiley & Sons: New York, 1988.
(20) Stern, E. A.; Newville, M.; Ravel, B.; Yacoby, Y.; Haskel, D. *Physica B* **1995**, *208/209*, 117.
(21) Newville, M.; Livins, P.; Yacoby, Y.; Rehr, J. J.; Stern, E. A. *Phys. Rev. B* **1993**, *47*, 14126.
(22) Zabinsky, S. I.; Rehr, J. J.; Ankudinov, A.; Albers, R. C.; Eller, M. J. *Phys. Rev. B* **1995**, *52*, 2995.
(23) Newville, M.; Ravel, R.; Haskel, D.; Rehr, J. J.; Stern, E. A.; Yacoby, Y. *Physica B* **1995**, *208/209*, 154.
(24) Chuchill, M. R.; Julis, S. A.; Rotella, F. J. *Inorg. Chem.* **1977**, *16*, 1137.
(25) Walz, L.; Scheer, P. *Acta Crystallogr., Sect. C* **1991**, *47*, 640.
(26) Farrugia, L. J. *J. Cluster Sci.* **2000**, *11*, 39.
(27) Farrar, D. H.; Grachova, E. V.; Lough, A.; Patirana, C.; Poe, A. J.; Tunik, S. P. *J. Chem. Soc., Dalton Trans.* **2001**, 2015.
(28) Deridder, D. J. A.; Imhoff, P. *Acta Crystallogr., Sect. C* **1994**, *50*, 1569.
(29) Singh, H. P. *Acta Crystallogr.* **1968**, *A24*, 469.
(30) Ricci, J. S.; Koetzle, T. F.; Goodfellow, R. J.; Espinet, P.; Maitlis, P. M. *Inorg. Chem.* **1984**, *23*, 1828.
(31) Cotton, F. A.; Kruczyns, L.; Shapiro, B. L. *J. Am. Chem. Soc.* **1972**, *94*, 6191.

Table 1. List of Reactions between $[Rh(1,5\text{-COD})Cl]_2$ and Different Substrates in the Kinetic Study of the Active Catalyst Formation

precatalyst	substrate	solvent	reaction no.	*T* (°C)	[Rh] (mM)	[substrate] (mM)	[substrate]/[Rh]	$t_{1/2}^{cat.}$ (min)	$t_{0.05}^{precip\ a}$ (min)
$[Rh(1,5\text{-COD})Cl]_2$	DMAB	toluene	1	25	3.7	120	32	7	–
			2		12	990	85	2	–
			3		12	450	37	17	36
			4		23	1900	84	8	80
			5		23	970	42	5	45
			6		23	490	21	10	19
			7		23	240	10	11	20
			8		26	850	33	15 (8)	24
			9	40	23	970	42	3.5	14
			10		23	240	10	6	9
		toluene	11	25	34	32	0.9	not converted	s
		THF	12		25	66	2.6	16 (13)	18
			13		23	980	42	6	50
$[Rh(1,5\text{-COD})Cl]_2$	AB	THF	14	25	24	920	39	1.3	2
			15		26	420	16	2	>6
$[Rh(1,5\text{-COD})Cl]_2$	CAB	toluene	16	25	23	20	0.9	n/a	s
			17		23	41	1.7	3.5	s
			18		23	460	20	<2	s
	DCAB		19		23	460	20	<2	s
	*t*BAB		20		21	450	22	<2	s
	DiPAB		21		24	770	31	60	s

[a] Time 5% Rh precipitates out of solution; s, soluble.

of spectra are available, the full principal components analysis (PCA) was not possible. In this case we used a simple empirical method that gives almost identical results in order to determine the reaction rate. The method entails finding the height difference between the maxima at 23 245 eV and the minima at approximately 23 270 eV.

In many cases the complex starts to precipitate in the later stages of the reaction. The XAFS edge height is proportional to the total amount of soluble rhodium in the X-ray beam (for a constant beam path length). Hence, the edge height provides an accurate measurement of the concentration of the soluble rhodium species that includes both the unreacted precatalyst and the soluble cluster. When rhodium-containing species precipitate, the edge height decreases proportionally due to the loss of the rhodium species.

3. Results

The formation of the catalyst must precede the amine borane dehydrocoupling reaction described in eq 1. The conversion of the rhodium-containing precursor compound, ($[Rh(1,5\text{-COD})Cl]_2$), to the rhodium cluster can be described by the sequence in eq 3.

We have also hypothesized[14] that, in the later stages of the reaction, a rhodium-containing material precipitates and that rhodium in the precipitate consists of small rhodium clusters that form a polymer-like product bonded by amine borane dimer in a reaction described in eq 4.

The goal of this work is to ascertain the details of these formation kinetics and then the structure of the important catalyst species and/or catalyst resting states. Using a variety of different XAFS methods we determine many different aspects of this reaction. First we use XAFS to follow the kinetics of formation of the predominant rhodium species. Evaluation of time-resolved XAFS spectra (1 min/spectrum) provides information about the rate of cluster formation and also about the number of rhodium species that are present during this reaction. We then use the XAFS spectra to determine the solubility of the cluster during the reaction from the measurement of the X-ray absorption edge height. We show that the solubility of the complex greatly diminishes in the later stages of the reaction for select amine

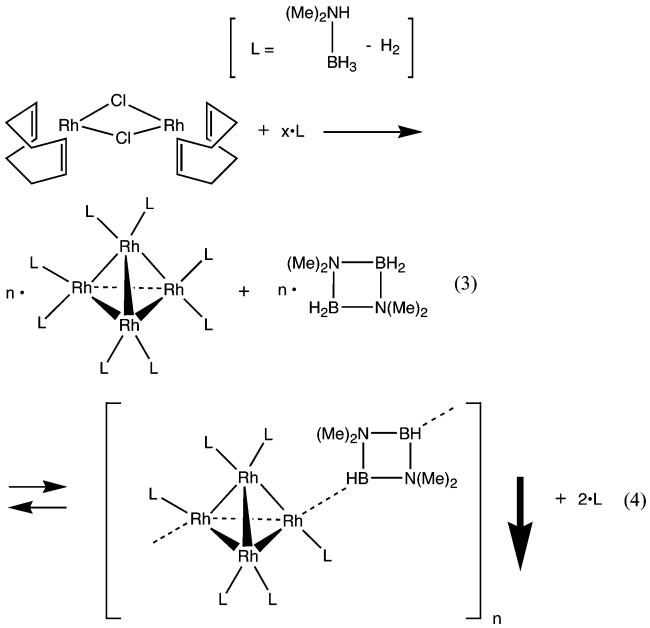

boranes but not for others. Finally we show how the same cluster forms from (i) different rhodium precursor compounds and from (ii) different amine borane compounds. This leads to the final determination of the cluster structure by fitting the XAFS spectra to theoretical standards.

3.1. Kinetics of the Rhodium Cluster Formation. 3.1.1. Factors Affecting the Reactions Rates and Principal Component Analysis of the Rhodium Cluster. A complete list of the reaction conditions used in the study is presented in Table 1. We found that a range of different alkyl amine borane compounds all convert the $[Rh(1,5\text{-COD})Cl]_2$ to a new species with very similar structures. This series of alkyl amine borane compounds include NH_3BH_3 (AB), Me_2NHBH_3 (DMAB), di-*i*PrNHBH$_3$ (DiPAB), *tert*-butylNH_2BH_3 (*t*BAB), $CyNH_2BH_3$ (CAB), and di-CyNHBH$_3$ (DCAB). Also shown in Table 1 are the $t_{0.5}^{cat}$ and $t_{0.05}^{precip}$ values that represent the time to convert 50%

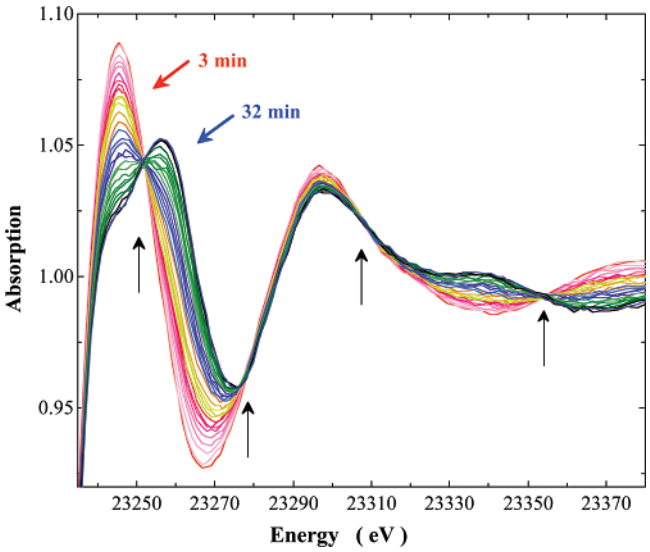

Figure 1. Time series of XAFS spectra above the Rh *K*-edge XAFS from 3 to 32 min for the reaction of DMAB with $[Rh(1,5\text{-}COD)Cl]_2$ in toluene at 25 °C (Table 1, reaction 3).

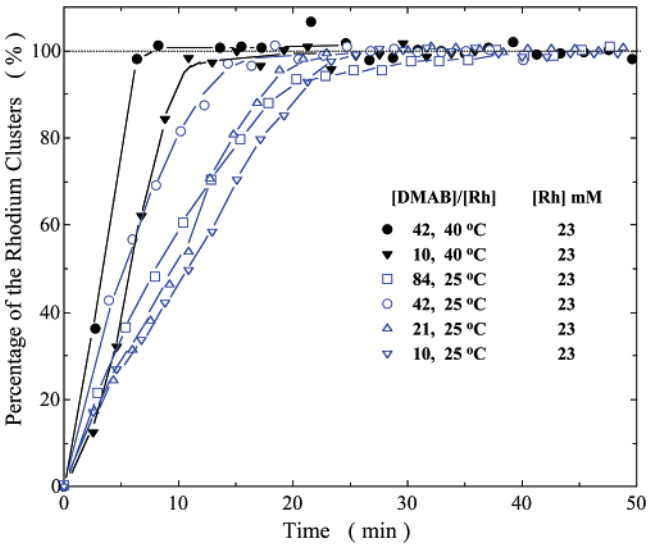

Figure 2. Concentration of the rhodium clusters as a function of time for DMAB in toluene at various concentrations as indicated. The complete conditions are listed in Table 1 for reactions 4−7, 10 and 11.

of the precursor to the new species and the time at which 5% of the rhodium complex have precipitated, respectively. The different amine borane compounds convert $[Rh(1,5\text{-}COD)Cl]_2$ to the new species at significantly different rates and to different extents. When all of the amine borane starting material has been consumed the rhodium complexes derived from AB and DMAB precipitate, whereas the complexes in contact with DiPAB, *t*BAB, CAB, and DCAB remain soluble. We also briefly explored other factors that affect reaction rates such as concentrations of the precatalyst and the amine borane substrate, temperature, and solvent type. These conditions are indicated in Table 1.

Figure 1 shows a time series of rhodium K-edge X-ray absorption spectra of the reaction of DMAB with $[Rh(1,5\text{-}COD)Cl]_2$ in toluene at 25 °C (Table 1, reaction 3) spanning the range from 23 230 to 23 380 eV that was typical of all the amine borane reactions with this catalyst precursor. The progression in the time series for the DMAB is very similar to that obtained for the other amine borane compounds, although rates of reaction were different according to the $t_{0.5}^{cat}$ values reported in Table 1. The primary feature of these spectra is the presence of a unique set of isosbestic points indicated by arrows in Figure 1. The presence of a unique set of isosbestic points[32] reveals the presence of two chemical states of rhodium as described by eq 3 in which the rhodium precursor is converted to *a single* catalytic form[33] (e.g., pure Rh_4 clusters or to a fixed ratio of mixed Rh_4/Rh_6 clusters as described later). We also conducted a principal components analysis (PCA) on this time series which showed that the spectra are a linear combination of the precatalyst and the new rhodium cluster spectra. PCA analysis also shows that no more than 2% of a third component could exist in this reaction series. Any transient species are present in negligible amounts. In addition, the XAFS analysis is not sensitive to the third shell atoms about the rhodium core. Hence changes in the ligands in the later stages of the reaction involving replacement of monomeric amine borane ligands with dimer or trimer amine borane products would not necessarily be detected.

3.1.2. Rh Cluster Formation Kinetics for AB, DMAB, CAB, DCAB, DiPAB. Figure 2 shows the rates of Rh cluster formation for DMAB in toluene under different reaction conditions described in Table 1 for reactions no. 4−7, 10, and 11. The $t_{0.5}^{cat}$ values for these reactions are also listed in Table 1. In most cases the amount of the new Rh cluster increases linearly with time. Most reactions had a significant excess of DMAB (see the [substrate]/[Rh] ratios), which means that the DMAB concentration does not change significantly over the course of the catalyst forming reaction. Higher DMAB concentrations and higher temperatures accelerate the formation of the Rh cluster.

The rate of formation of the Rh cluster for AB in THF is almost 5 times faster than that for DMAB under the same conditions (Figure 3 and reactions 13 and 14 in Table 1). Likewise CAB has a Rh cluster formation rate that is over 5 times faster than that for DMAB with the same solvent and temperature conditions (reactions 6 and 18). The rate data for CAB and DiPAB (reactions 19 and 21) show a much different behavior than those for the other systems. There appear to be two different mechanisms involved: a rapid rate at times less than about 10 min and then a very slow conversion over several hours to the final state. This is consistent with the steric bulk of these di-substituted amine boranes especially if two (or more) of these are ligands on each rhodium atom in the cluster. The first ligation will have less steric interaction compared to the ligation of the second amine borane. The rate of cluster formation increases as AB ≈ CAB ≈ *t*BAB > DMAB > DCAB ≈ DiPAB.

3.2. Solubility of the Rhodium Clusters. 3.2.1. Precipitation during Reaction. In the later stages of the reaction the rhodium clusters precipitate for AB and DMAB although to different extents. Figures 4 and 5 show the percentage of soluble rhodium with time under different reaction conditions for DMAB and AB. The decrease in rhodium absorbance is the direct result of the precipitation of the rhodium complex. To quantitatively

(32) Senior, W. A.; Verrall, R. E. *J. Phys. Chem.* **1969**, *73*, 4242.
(33) We realize that one cannot ever rule out very small amounts of unobservable species being the actual catalyst. We also realize that what we are calling the catalyst may in fact be a resting state of the actual catalyst. However the structure of this resting state most likely has an impact on the actual catalyst species.

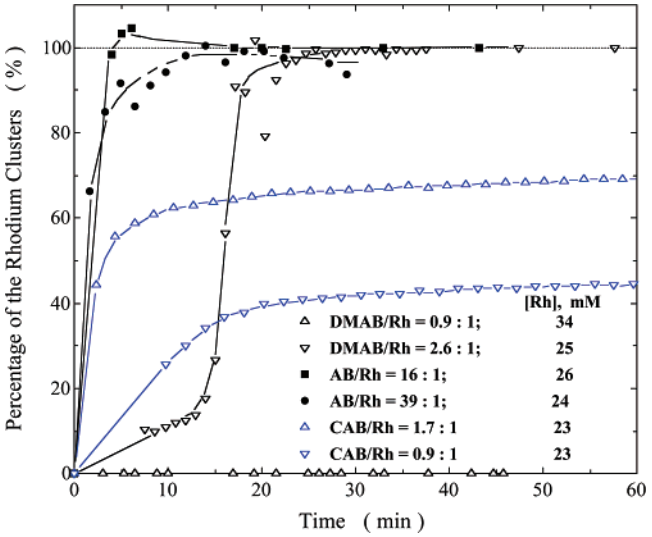

Figure 3. Concentration of the rhodium clusters as a function of time for DMAB, AB, and CAB at various concentrations as indicated. The complete conditions are listed in Table 1 for reactions 11, 12, 14, 15, 16, and 17. All reactions conducted in THF except for DMAB/Rh = 0.9:1 that was conducted in toluene.

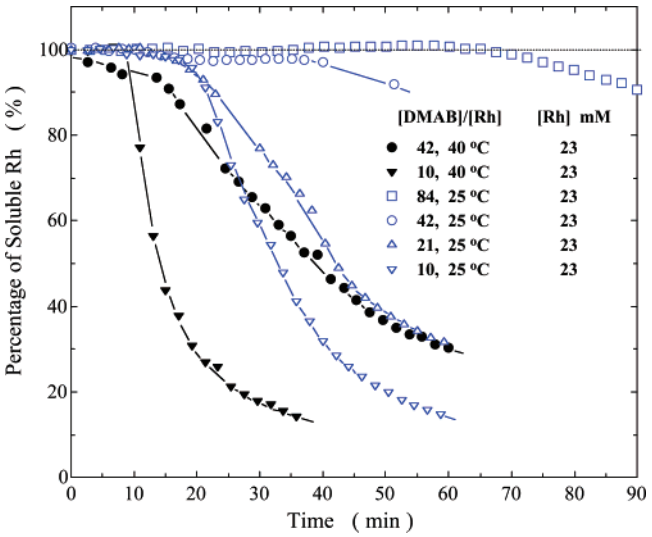

Figure 4. Solubility of the rhodium clusters as a function of time for DMAB in toluene at various concentrations as indicated. The complete conditions are listed in Table 1 for reactions 4−7, 10, and 11.

compare this effect, Table 1 lists the $t_{0.05}^{\text{precip}}$ value that is the time at which 5% of the rhodium clusters precipitate. After the initial rapid rate of precipitation, the soluble rhodium species decreases until it reaches a saturation concentration. For higher DMAB concentrations the saturation concentration of the Rh cluster appears to be much higher, although this might reflect the higher solubility of Rh clusters with appended DMAB monomer vs dimer ligands. The system containing AB in THF undergoes rapid catalyst precipitation at an early stage and exhibits a much lower solubility of the active form.

The rhodium complex, generated from DiPAB, *t*BAB, CAB, and DCAB, remains soluble throughout the reaction; hence the nature of the ligand appended to the rhodium core plays an important role in its solubility. The amine borane oligomeric species formed have multiple sites of binding to the rhodium cluster (see eq 4) that can lead to formation of polymeric structures. The amine borane compounds with a bulky alkyl

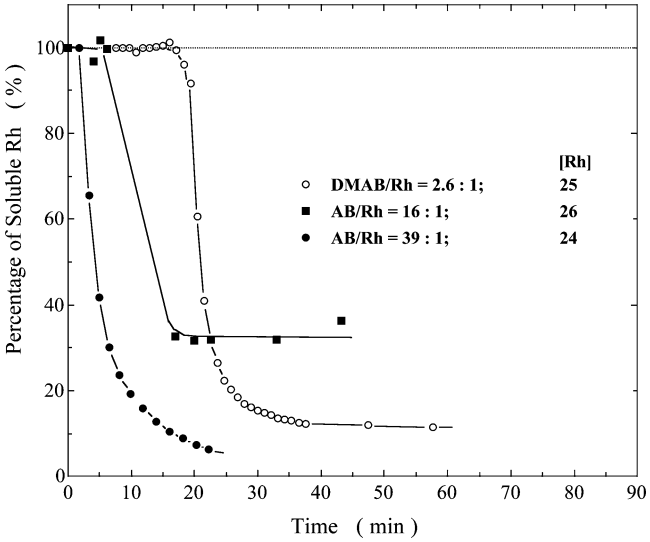

Figure 5. Solubility of the rhodium clusters as a function of time for DMAB and AB in THF at various concentrations as indicated. The complete conditions are listed in Table 1 for reactions 12, 14, and 15. Concentration of Rh is in mM.

group may be more inhibited toward polymer formation due to steric effects. Alternatively the alkyl groups on the nitrogen may increase the solubility of the rhodium catalyst complex over the methyl or hydrogen found on DMAB and AB. These arguments are consistent with the highest precipitation rate observed for AB that ultimately forms a trimer (borazine) or a polymer (polyborazalene) having three binding sites with minimal steric hindrance.

3.2.2. Precipitation or Redispersion of Rhodium Clusters by Adding DMAB Dimer or Monomer. The addition of DMAB dimer to the catalytic system clearly hastens precipitation of the rhodium complex, Figure 6a. In contrast the addition of DMAB monomer to the precipitate at the very end of reaction 5 (Table 1), Figure 6b illustrates the redissolution of the precipitate with the production of hydrogen gas and more DMAB dimer. *This latter result indicates that the precipitate is not a metal or metal nanoparticle since it is unlikely that simple replacement of the ligand could lead to breakup of the metal−metal bonds.* The observation of the precipitated rhodium complex catalyzing the dehydrocoupling of amine boranes may lead to the assumption of the operation of a heterogeneous catalyst due to the dark opaque color of the solution.

3.3. XAFS Spectra of the Rhodium Clusters. 3.3.1. Preliminary Examination of the Rhodium Coordination Structure and the Effect of Solvent Type. The uncorrected, *k*- and k^2-weighted $|\tilde{\chi}(R)|$ plots for the predominant rhodium species are shown in Figure 7a and 7b. The $|\tilde{\chi}(R)|$ functions are generated by Fourier transformation of the XAFS spectrum represented in the form of $\chi(k)$ as defined in eq 2. The $|\tilde{\chi}(R)|$ plots represent the partial pair distribution (ppd) functions convoluted with the photoelectron scattering functions shown in eq 2. The plots approximately represent the probability of finding a certain type of neighboring atom about the central X-ray absorbing atom. The peak widths are artificially broadened from the true ppd functions since the phase of the oscillations for a certain scattering atom is dependent upon *k* which is not the case for classical X-ray diffraction. Likewise the peak positions in Figure 7 are before the phase correction and are thus typically shorter by about 0.2−0.4 Å from the true position.

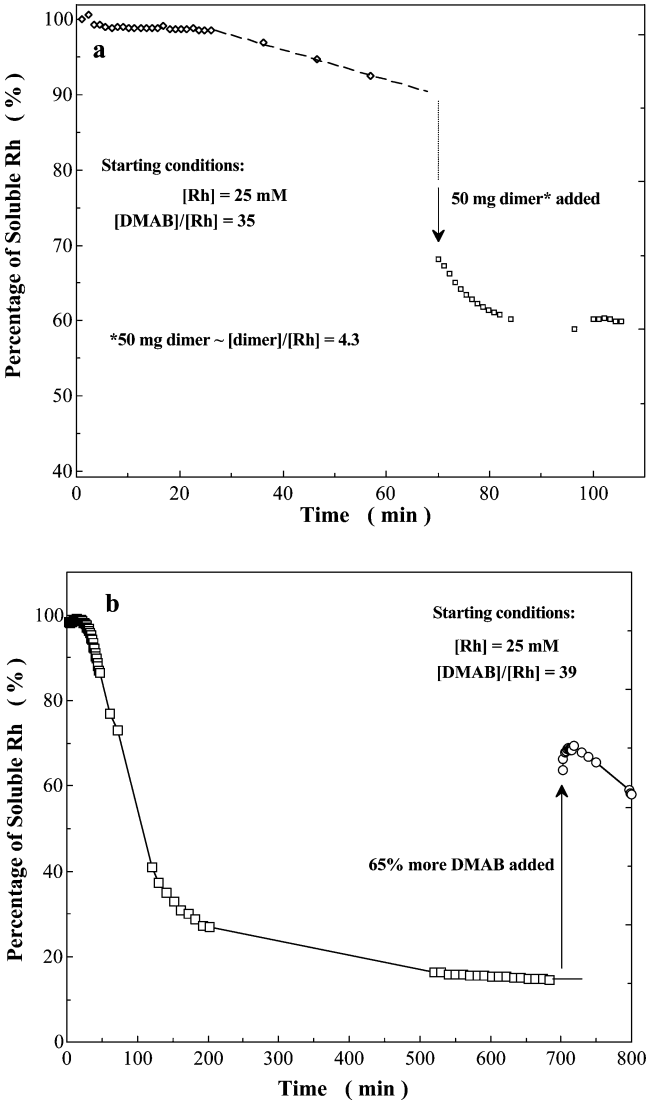

Figure 6. (a) Precipitation of rhodium clusters upon addition of the cyclic dimer product from the DMAB reaction. Reaction involving the precursor, $[Rh(1,5\text{-}COD)Cl]_2$, in toluene at 25 °C. (b) Dissolution of the spent catalyst upon addition of DMAB in toluene at 25 °C.

However, the complex phase shift relationship for different atoms is accurately predicted by FEFF so that the true peak positions *and* widths are recovered later in the fitting process. It is important to evaluate both the magnitude ($|\tilde{\chi}(R)|$) and imaginary ($\mathrm{Im}[\tilde{\chi}(R)]$) portions of the Fourier transforms since both components are required to capture all the information contained in the original XAFS spectra. It is also instructive to evaluate both k- and k^2-weighted $|\tilde{\chi}(R)|$ since the latter enhances the peak heights of higher Z atoms such as rhodium. Examples shown in the Supporting Information graphically illustrate the ability of XAFS to clearly discriminate rhodium atoms in the first shell from the second row elements such as B, C, or N located at nearby positions.

Figure 7 provides the $\tilde{\chi}(R)$ plots for the predominant rhodium species generated from $[Rh(1,5\text{-}COD)Cl]_2$ with DMAB in toluene at 25 °C corresponding to reaction 6 in Table 1. The main features are the two peaks located near 1.6 and 2.4 Å, corresponding to first-shell boron (most probable assignment, described later) and rhodium atoms, respectively. $[Rh(1,5\text{-}COD)Cl]_2$ rapidly reacts ($t_{0.5}^{cat} = 10$ min) to form the final rhodium

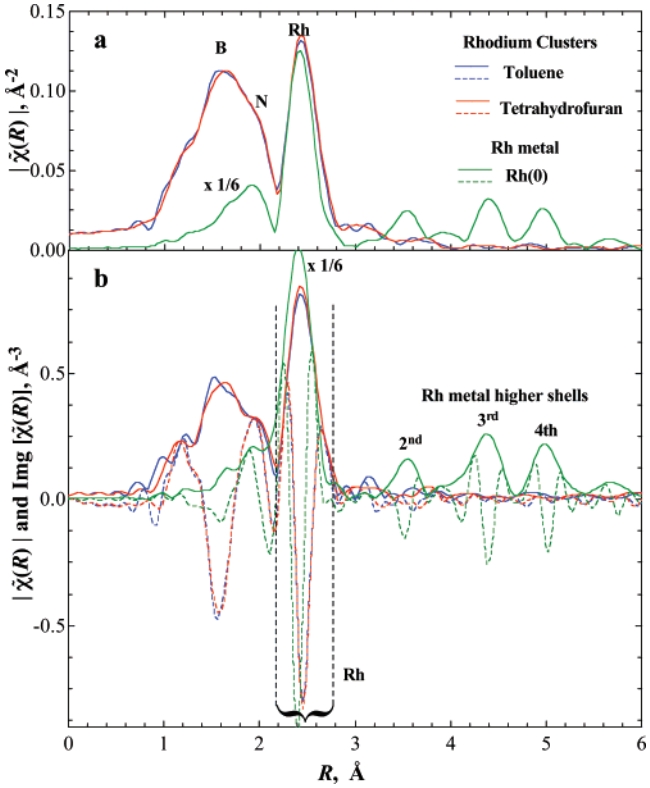

Figure 7. (a) k-weighted $|\tilde{\chi}(R)|$ plots for the rhodium clusters in both toluene and tetrahydrofuran using the precursor, $[Rh(1,5\text{-}COD)Cl]_2$. (b) k^2-weighted $|\tilde{\chi}(R)|$ (solid lines) and $\mathrm{Im}[\tilde{\chi}(R)]$ (dashed lines) plots for the rhodium clusters. A rhodium metal foil spectrum is also included that has been scaled by $^1/_6$ for comparison to the active catalyst spectra. In all cases the k range for the Fourier transform is 2−17 Å^{-1}. Distances are not corrected for photoelectron phase shifts.

species that is identified by the intense new peak occurring at 2.4 Å (see Supporting Information for $|\tilde{\chi}(R)|$ of the precursor). This peak can be uniquely assigned to rhodium−rhodium bonds by examining the shape of the $\mathrm{Im}[\tilde{\chi}(R)]$ portion of the transform in Figure 7b between 2.2 and 2.8 Å. This "signature" of rhodium scattering does not occur for boron or nitrogen atoms (see Supporting Information). Also shown in Figure 7 is the spectrum of the rhodium species produced in THF (Table 1, experiment 13) which is identical in every respect to that produced in toluene. Thus the primary role of the solvent for this reaction is to mediate the solubility of the reactants, products, and the rhodium complexes.

Also shown in Figure 7 is the $|\tilde{\chi}(R)|$ data for metallic rhodium in which the spectrum has been scaled by $^1/_6$ to better compare to the rhodium species produced with DMAB. The much greater intensity of the peak at 2.4 Å is a result of 12 nearest rhodium neighbors in the metallic form versus approximately 3 nearest neighbors observed for the new rhodium species. (After phase correction the rhodium−rhodium distance for metal is 2.68 Å, and as shown in the Supporting Information, the distances for the first through fourth rhodium shells are within 0.005 Å of the XRD values.) The other significant features of the metallic rhodium spectrum are the peaks at 3.6, 4.4, and 5.0 Å corresponding to the second, third, and fourth rhodium shells, respectively. In the $\mathrm{Im}[\tilde{\chi}(R)]$ portion of the transform these satellite peaks appear as an abrupt series of oscillations that are unique to only rhodium−rhodium scattering paths. These satellite peaks are completely absent in the rhodium species

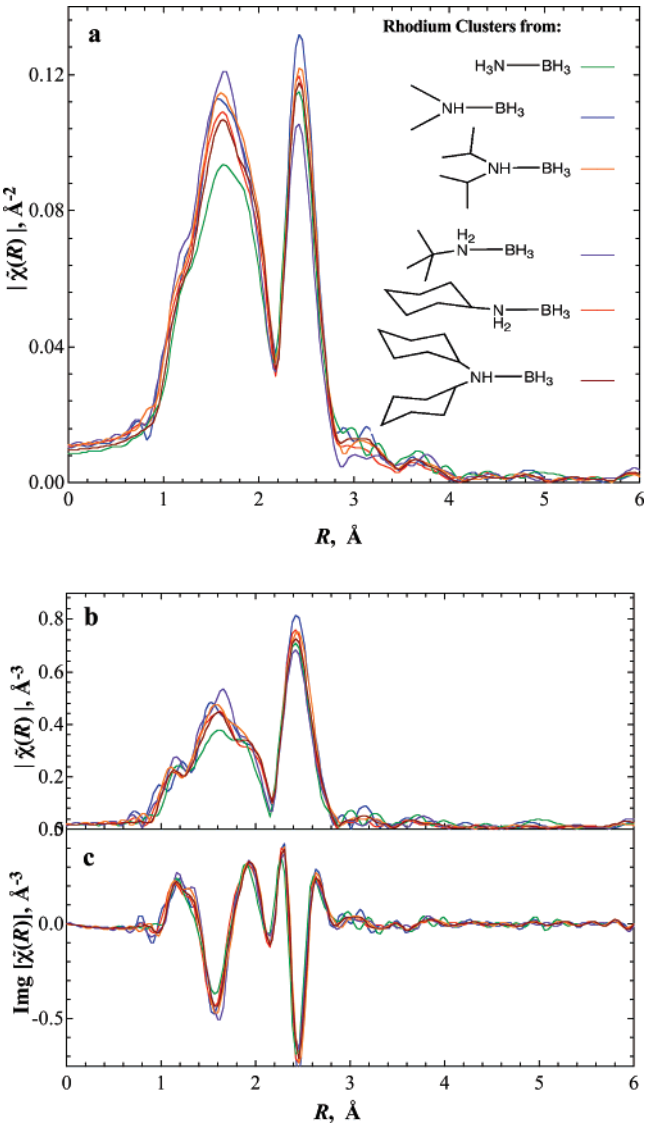

Figure 8. (a) k-weighted $|\tilde{\chi}(R)|$ plots for the rhodium clusters generated from a series of alkyl amine borane compounds as shown starting from the precursor, $[Rh(1,5\text{-}COD)Cl]_2$. (b) k^2-weighted $|\tilde{\chi}(R)|$ and (c) $Im[\tilde{\chi}(R)]$ plots for the rhodium clusters. In all cases the k range for the Fourier transform is 2−17 Å^{-1}. Distances are not corrected for photoelectron phase shifts.

produced with amine boranes showing that the predominant rhodium species does not contain higher rhodium shells.

3.3.2. Structure of the Rhodium Clusters Synthesized from AB, DMAB, DiPAB, *t*BAB, CAB, and DCAB. The various alkyl amine borane compounds all convert $[Rh(1,5\text{-}COD)Cl]_2$ to nearly the same rhodium cluster with different conversion times according to the $t_{0.5}^{cat}$ values given in Table 1. Figure 8a and 8b show the various $\tilde{\chi}(R)$ plots for this series of alkyl amine boranes including AB and the primary and secondary amine boranes. The first and second shell atoms of the amine borane ligands that bond to rhodium are nearly identical for all the alkyl amine boranes. This similarity suggests, but does not prove, that the amine borane or oligomeric product bonds to rhodium through the boron atom rather than through the amine nitrogen. If the nitrogen was bound directly to the rhodium then the differences in the number and type of alkyl groups would contribute different intensities to the second-shell portion of the $\tilde{\chi}(R)$ plots in the region from approximately 1.6 to 2.2 Å.

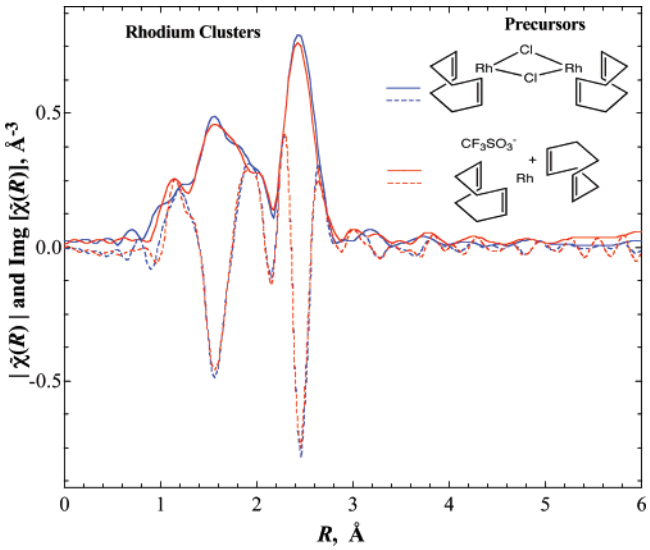

Figure 9. k^2-weighted $|\tilde{\chi}(R)|$ and $Im[\tilde{\chi}(R)]$ plots for the rhodium clusters from two different precursors, $[Rh(1,5\text{-}COD)Cl]_2$ and from bis(1,5-cyclooctadiene)rhodium (I) trifluoromethane sulfonate. The k range for the Fourier transform is 2−15 Å^{-1}. Distances are not corrected for photoelectron phase shifts.

However since no significant differences in the second shell structure are detected it appears that rhodium binds to boron. Hydrogen cannot be detected using XAFS.

3.4. XAFS Spectra of the Rhodium Clusters from Various Precursors. 3.4.1. Chloro-(1,5-cyclooctadiene)rhodium (I) Dimer, Bis(1,5-cyclooctadiene)rhodium (I) Trifluoromethane-sulfonate. Figure 9 shows the k^2-weighted $|\tilde{\chi}(R)|$ plot of the rhodium cluster species generated from two different starting precursors. The first precursor has one cyclooctadiene and two chloride ligands, while the latter compound has two cyclooctadiene ligands and an outer shell triflate ion ($CF_3SO_3^-$). The XAFS spectra of these two precursor materials are significantly different (see Supporting Information), and yet the rhodium complexes produced from these two compounds are nearly identical. The transformed spectra of the rhodium complex are identical in all respects in both the $|\tilde{\chi}(R)|$ and $Im[\tilde{\chi}(R)]$ plots. The 1,5-cyclo-octadiene ligands are displaced during the reaction and hydrogenated under these conditions to produce cyclooctane as determined by GC and NMR. The similarity of the rhodium complexes produced from the two precursors conclusively shows that Cl^- no longer resides in the first coordination shell. As a third row element, a Cl^- ion provides a strong back scattering signal that produces a distinct peak in the $|\tilde{\chi}(R)|$ plot at about 2 Å (e.g, see spectrum of $[Rh(1,5\text{-}COD)Cl]_2$ in the Supporting Information).

3.4.2. XAFS Spectra of the Rhodium Complex from Other Precursors. Four other precursor materials were studied including three different carbonyl compounds and a pentamethyl cyclopentadienyl complex. The spectrum of the rhodium clusters from each of these different precursors is shown in Figure 10. There is a remarkable transition for all six different precursors in this study to a common form containing a rhodium cluster core. Four of the precursor compounds shown in Figures 9 and 10 have no first shell rhodium−rhodium bonds resulting in very diverse spectra (the Supporting Information compares the precursor to its final form) due to the different ligand types and coordination numbers. On the other hand, these four different precursors undergo a transition to a structure with a nearly

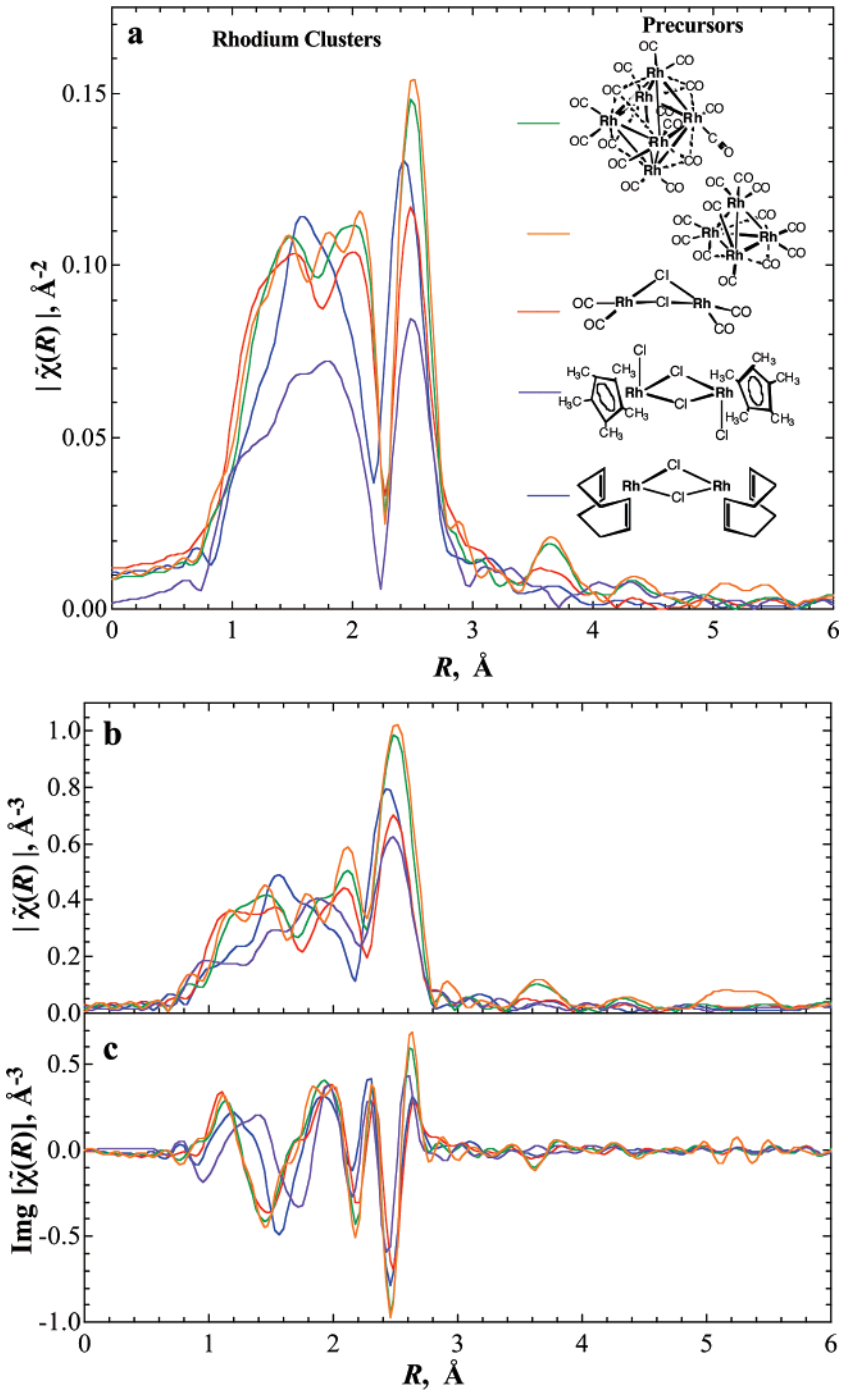

Figure 10. (a) *k*-weighted $|\tilde{\chi}(R)|$ plots for the rhodium clusters derived from different precursor compounds including Rh_6CO_{16} ($T = 40$ °C in toluene, $t =$ 20 h), $Rh_4(CO)_{12}$ ($T = 40$ °C in THF, $t = 13$ h), $[Rh(CO)_2Cl]_2$ ($T = 40$ °C in toluene, $t = 13$ h), a pentamethyl cyclopentadienyl complex ($T = 40$ °C in toluene, $t = 2$ h), and $[Rh(1,5\text{-COD})Cl]_2$. (b) k^2-weighted $|\tilde{\chi}(R)|$ and (c) $\text{Im}[\tilde{\chi}(R)]$ plots for the rhodium clusters from the various precursors. The *k* range for the Fourier transform is $2-15$ Å^{-1}. Distances are not corrected for photoelectron phase shifts.

identical rhodium cluster but with some slight differences in the ligand structure as shown in Figures 9 and 10. $Rh_6(CO)_{16}$ and $Rh_4(CO)_{12}$ already exist with the basic rhodium cluster core. In these cases, the reaction with the amine borane is mostly a ligand substitution reaction, displacing at least some of the strongly binding CO ligands. As shown in Figure 10, these carbonyl compounds have slightly different structures in the range from 1 to 2 Å. Model fitting shows that the ligands are likely a mixture of CO and amine borane compounds.

3.4.3. XAFS Spectra of the Precipitate. The solution quickly becomes opaque black shortly after mixing the amine borane solution with the precatalyst solution. In the later stages of the reaction, precipitation of a rhodium-containing species occurs when the reactions are carried out with DMAB or AB (see Table 1). After several hours to days, depending on solvent and amine borane-to-rhodium ratios, the supernatant is clear and the black material settles to the bottom of the reaction vessel. For these solutions there is no coating of the glass reactor with rhodium complex, and these surfaces remain optically and spectroscopically clear. Hence all of the insoluble rhodium species remains in the precipitated material. By conducting XAFS measurements on this precipitate it is possible to evaluate the rhodium structure

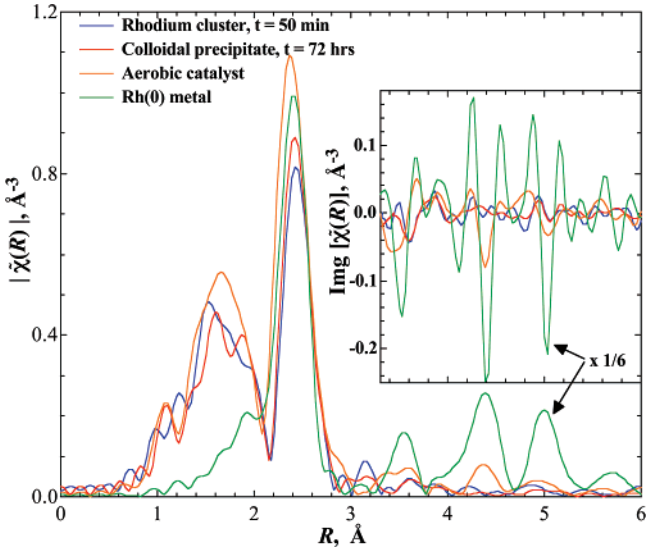

Figure 11. k^2-weighted $|\tilde{\chi}(R)|$ plots for various forms of the rhodium clusters derived from the precursor, $[Rh(1,5\text{-}COD)Cl]_2$ with DMAB in toluene at 25 °C. The inset shows the corresponding k^2-weighted $\mathrm{Im}[\tilde{\chi}(R)]$ in the range from 3.3 to 6 Å. The k range for the Fourier transform is 2−17 $Å^{-1}$. Distances are not corrected for photoelectron phase shifts.

in this material and also to explore the possibility of the presence of a trace amount of a metal phase.

In Figure 11 we compare the k^2-weighted $|\tilde{\chi}(R)|$ plots for the rhodium complex produced with DMAB at $t = 0.8$ h with the precipitate that was anaerobically recovered after 72 h under reaction conditions. The precipitate shows similar XAFS characteristics to the soluble rhodium complex. For comparison, the spectra of metallic rhodium is also shown and is scaled by a factor of $^1/_6$. The precipitate shows no evidence of the higher rhodium−rhodium shells at 3.6, 4.4, and 5.0 Å. This is especially clear in the expanded view of the $\mathrm{Im}[\tilde{\chi}(R)]$ plots shown in the inset of Figure 11. Thus, within the detection limits, we can conclude that less than 1% of the rhodium precipitate could be in the metallic form at this stage. This material has *virtually no* tendency, in a reducing environment (H_2 saturated) or under a nitrogen atmosphere, to convert to the metal over long time periods. The ligands apparently stabilize the cluster and inhibit reduction to the metal form.

Another dehydrocoupling reaction of DMAB was conducted under aerobic conditions in a sample cell designed to readily allow air exchange at the surface of the reacting mixture. The cell was an open plastic trough of essentially the same dimensions as the glass vials. In both the $|\tilde{\chi}(R)|$ and $\mathrm{Im}[\tilde{\chi}(R)]$ plots in Figure 11 we see clear evidence that the precipitate from this reaction contains metallic rhodium with higher rhodium−rhodium shells that match the peaks at 3.6, 4.4, and 5.0 Å for bulk metal. From the amplitudes of these peaks we can estimate that about 5% of the total rhodium is in a metallic state. This counterintuitive observation can be rationalized by the oxidation of the borane ligands to borates (which is observed by ^{11}B NMR). Presumably some of the cluster reacts with O_2 according to eq 5.

$$[Rh(1,5\text{-}COD)Cl]_2 + \mathrm{DMAB\ (excess)} \rightarrow [Rh(BH_2NHMe_2)_2]_4 + O_2 \rightarrow Rh_{metal} + nB_xO_y + 8NHMe_2 \quad (5)$$

Additional evidence for this reaction is the strong aroma of dimethylamine from the reaction mixture upon long exposure

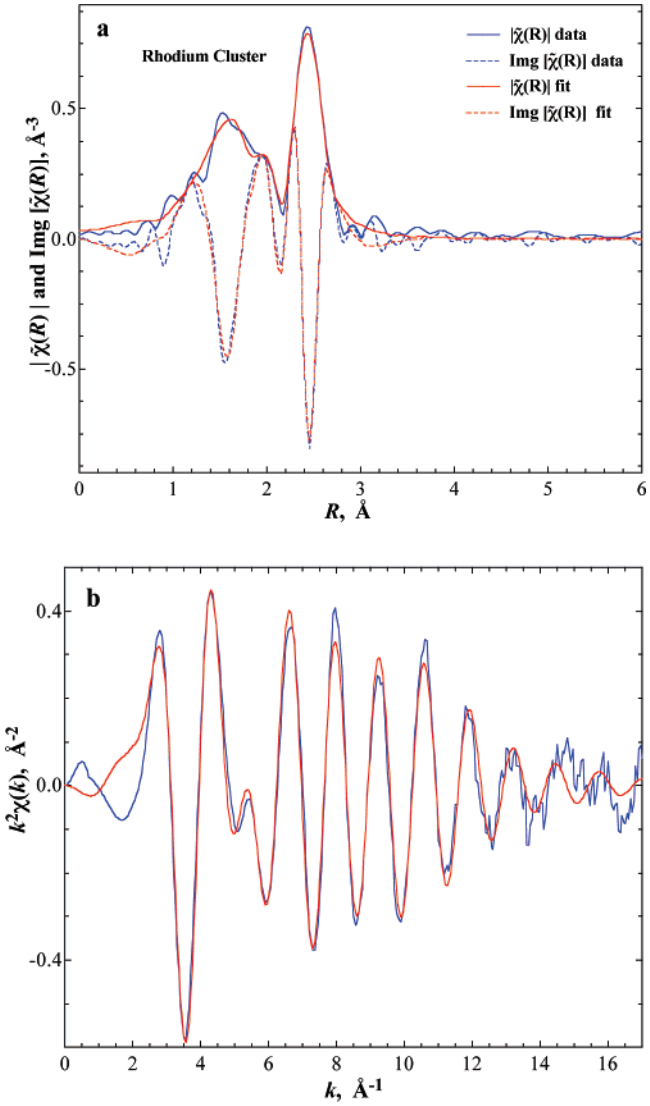

Figure 12. (a) k^2-weighted $|\tilde{\chi}(R)|$ and $\mathrm{Im}[\tilde{\chi}(R)]$ plots for the rhodium clusters derived from the precursor, $[Rh(1,5\text{-}COD)Cl]_2$ with DMAB in toluene at 25 °C. The fitted lines are results from the FEFF8 standard and parameters listed in Table 2. (b) Rh XAFS k^2-weighted $\chi(k)$ plots for Rh solution. The experimental data and the model fit are shown.

to air while a recently opened solution has virtually no odor. Thus in the presence of air, the rhodium catalyst can be converted to metal. We have also observed metallic rhodium when an anaerobic precipitate was exposed to air. This leads to an important point, that incorrect results could be obtained by *ex situ* meausurements involving transporting material into the analytical instruments, e.g., TEM or XPS, without rigorously excluding O_2.

3.5. Structural Parameters of the Rhodium Cluster from XAFS Analysis. Quantitative information about the cluster structure is obtained by fitting the experimental data to the FEFF8 theoretical standards.[20,23] Figure 12a and 12b show the $\tilde{\chi}(R)$ and $\chi(k)$ plots of both the fits and the experimental data for the rhodium clusters generated from DMAB in toluene at 25 °C. In all cases there is an excellent fit to the experimental data. Table 2 provides the structural parameters that were derived from these fits including the coordination numbers and distance for atoms in the first and second shells about a central rhodium atom. The rhodium−rhodium bond distances are 2.734 ± 0.005 Å which are somewhat longer than the rhodium−

Table 2. Results of the XAFS Analysis of the Rhodium Clusters at 25 °C[a,d]

solution	ID	bond	N	R (Å)	σ^2_{SS} ($\times 10^{-3}$ Å^2)	E_0	$\mathscr{R}$ [b]
$[Rh(1,5\text{-COD})Cl]_2$	1	Rh−Rh	3.3 (0.3)	2.734 (0.005)	8.2 (0.6)	−2.4	0.03
		Rh−B	2.2 (0.4)	2.095 (0.019)	6.3 (2.3)		
		Rh−N	2.2[c]	2.67 (0.04)	16.1 (7.4)		

[a] For the fit, k^2-weighting is applied, where σ^2_{SS}, is the Debye−Waller factors for the single scattering path. Uncertainty is given in parentheses. In all cases the k range used in the transform was from 2 to 17 Å^{-1}. [b] Goodness of fit defined by a scaled sum of squares as described in FEFFIT.[23] [c] Fixed to the Rh−B value [d] Reported uncertainties for all parameters based upon the method described in FEFFIT.[23]

rhodium distance of 2.68 Å in bulk metal. The rhodium−rhodium coordination number is 3.3 ± 0.5 which implies that the average rhodium cluster contains approximately four rhodium atoms (the coordination number uncertainty, ±0.5, is derived from the estimate of S_0^2 and eq 2). Each rhodium atom is ligated with approximately two boron atoms having a rhodium−boron distance of 2.095 Å. More details of the fitting procedure are given in the Discussion section.

4. Discussion

4.1. Structure of the Rhodium Core. 4.1.1. Rhodium Cluster Coordination Number. For all rhodium precursors and all the amine borane substrates examined in this study, the XAFS results strongly suggest that the rhodium complex produced consists of a small cluster composed of a few rhodium atoms with a ligand shell. There are uniquely different features of the XAFS spectra that place certain constraints on the maximum size of this cluster. To demonstrate the sensitivity of XAFS to determine the cluster size, it is necessary to evaluate the method using known standards. Three of the rhodium precursor compounds, $[Rh(1,5\text{-COD})Cl]_2$, $[Rh(CO)_2Cl]_2$, and $[Cp^*RhCl_2]_2$, are dimers that contain no rhodium in the first shell but that have a single rhodium in the second shell. In each spectrum there is an unambiguous backscattering signal from rhodium in this second shell (see Figures S9, S10, and S11 in the Supporting Information). For $Rh_6(CO)_{16}$, each rhodium atom has four first-shell rhodium atoms and a single second-shell atom. The XAFS spectrum of this compound also clearly shows the existence of the single rhodium atom in the second shell (see Figure S8). Rh(0) metal has a face centered cubic structure in which there are 12 rhodium atoms in the first shell, 6 in the second shell, 24 atoms in the third shell, and 12 atoms in the fourth shell. As shown in Figure 7a, the $\tilde{\chi}(R)$ plots for the Rh-(0) metal show that the peaks assigned to the third and fourth shells at 4.4 and 5.0 Å are *more intense* than that of the second shell at 3.6 Å due to the higher coordination numbers in these shells. When the properties of these five standards are compared to the new rhodium complex spectrum in Figure 7, several conclusions are possible. The new complex shows no evidence of backscattering from either the third or fourth rhodium shells that would be indicative of metallic rhodium or rhodium nanoparticles. On the other hand, in Figure 7 there is possibly some scattering signal corresponding to the peak at 3.6 Å. However the intensity of this peak is only about 20% of the intensity for a Rh_6 cluster such as $Rh_6(CO)_{16}$ that is shown in Figure 10a. One possibility is that there is an equilibrium between two relatively stable cluster sizes of Rh_4 and Rh_6 as shown in eq 6. If we assume a simple equilibrium model of 80% Rh_4 in equilibrium with 20% Rh_6 based upon the intensity of the peak at 3.6 Å, the calculated coordination number would be 3.2 which is very close the coordination number of 3.3

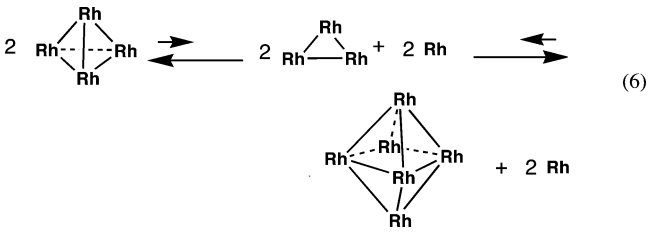

(6)

measured *independently* from the main first shell peak at 2.4 Å. Alternatively the two clusters Rh_4 and Rh_6 are produced in the same 4:1 ratio throughout the reaction.

4.1.2. Rhodium−Rhodium Bond Distance in the Rhodium Cluster. As shown in Figure 13, small metal clusters, which have no external ligands, undergo a bond contraction as cluster size becomes smaller wherein the degree of bond contraction follows an approximately $n^{-1/3}$ relationship (n is the number of atoms).[34] This shrinking occurs as a result of minimizing the surface free energy. At the two extremes, the metal−metal bond distance for a metal dimer is typically about 0.2−0.3 Å shorter than that for bulk metal for metals such as Pt, Cu, Au, and Ir.[34−37] In contrast, the Rh_{4-6} cluster in this study has a rhodium−rhodium bond distance (2.73 Å) that is about 0.04 Å *longer* than that for bulk metal (2.69 Å). This indicates that the bonding with ligands leads to transfer/sharing of valence electrons with the ligands that cause a weakening of the bonding between the rhodium atoms, giving rise to a longer rhodium−rhodium bond distance.

Other stable rhodium clusters have a longer bond distance than that for bulk metal. As illustrated in Figure 13, $Rh_6(CO)_{16}$ has a rhodium−rhodium bond distance of 2.749 Å[27] (or 2.754 Å from XAFS, Supporting Information) and $Rh_4(CO)_{12}$ has an average bond distance of 2.71 Å.[26] These ligands are capable of stabilizing these clusters, and in so doing the rhodium−rhodium bond distances are longer than that for bulk metal, an indication that the ligands have overcome the high surface free energies. Therefore the long rhodium−rhodium bond length for the amine borane ligated Rh_{4-6} cluster strongly suggests that the rhodium core is stabilized against agglomeration to metallic particles or nanoparticles.

4.1.3. Are Rh Metal Nanoparticles Present during Reaction? The evidence is quite strong that the vast majority of the rhodium is converted to Rh_{4-6} clusters during the active part of the catalytic dehydrocoupling reaction. There is also important evidence that little, if any, nanoparticle or bulk metal phase is present.

(34) Ankudinov, A. L.; Rehr, J. J.; Low, J. J.; Bare, S. R. *J. Chem. Phys.* **2002**, *116*, 1911.
(35) Montano, P. A.; Shenoy, G. K.; Alp, E. E.; Schulze, W.; Urban, J. *Phys. Rev. Lett.* **1986**, *56*, 2076.
(36) Haberlen, O. D.; Chung, S. C.; Stener, M.; Rosch, N. *J. Chem. Phys.* **1997**, *106*, 5189.
(37) Ferrari, A. M.; Neyman, K. M.; Mayer, M.; Staufer, M.; Gates, B. C.; Rosch, N. *J. Phys. Chem. B* **1999**, *103*, 5311.

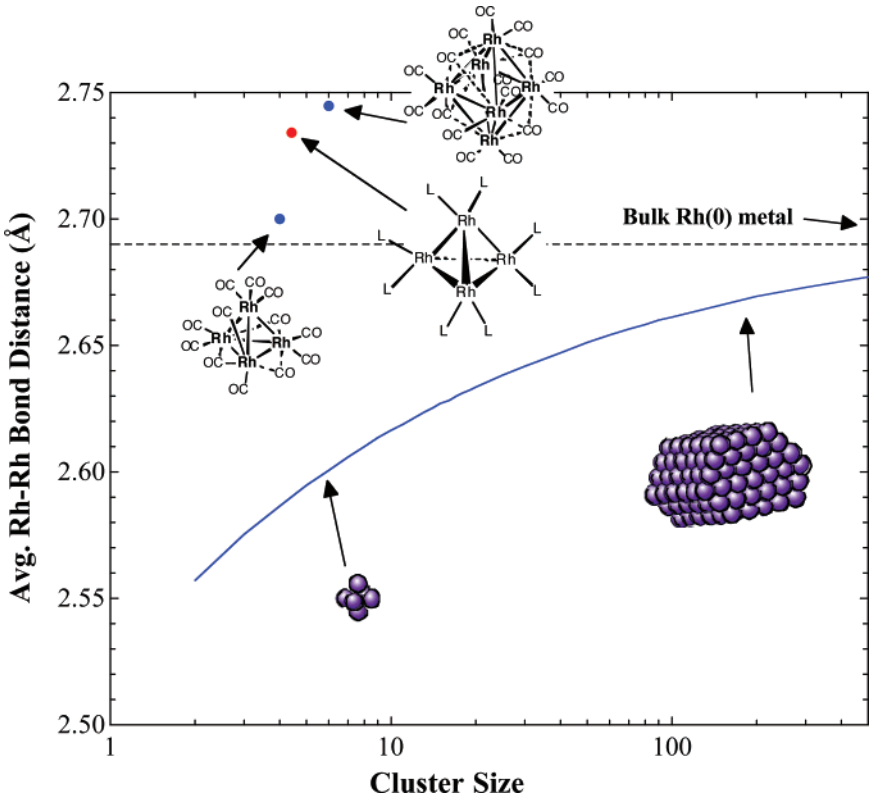

Figure 13. Average rhodium−rhodium bond length for metal clusters having no ligands ($n^{-1/3}$ relationship) and for various organometallic rhodium clusters in this study.

The measured rhodium−rhodium coordination number is 3.3. For low coordination number the XAFS uncertainties on the measured cluster size are small. Frenkel[38] reported a comprehensive study of platinum nanoparticles looking at the effect of size and shape on the XAFS spectra. When the measured first shell coordination number is less than about 6, accurate measurements of the cluster size are possible. As the coordination number asymptotically approaches the bulk metal value of 12, the precision for the measured nanoparticle size is greatly diminished. The smallest platinum nanoparticle in the Frenkel study was 2.4 nm with a measured first shell coordination number of 8.5 (XAFS). For this small cluster, scattering contributions from the second, third, and fourth shells are still clearly evident. In other words, for a 2.4 nm particle the $\tilde{\chi}(R)$-peaks in the range from 3 to 6 Å have amplitudes that remain at about 20% of the amplitude of the first shell peak at 2.5 Å. In a study of small 13 atom Cu clusters, the scattering from the second and third shell metal was clearly detected.[35] For the rhodium cluster of this study there is no evidence of higher shells in the 3 to 6 Å range. Hence this analysis is consistent with the fact that the cluster size is about four atoms since the higher shell scattering is not present. Further, for the active catalyst system it is possible to evaluate both the magnitude and the imaginary $\tilde{\chi}(R)$ peaks in the range from 3 to 6 Å to establish an upper limit for the presence of trace metal (nanoparticles or bulk) of <1%.

The spectrum of the precipitate after 72 h in an H_2 environment provides another important test for the existence of a trace metal nanoparticle species. The transition from the precursor compound to a nanoparticle phase should progress through the rhodium cluster stage. We can consider two different classes of ligand types. One would be described as a *weak* ligand wherein the free energy of the metal nanoparticle is lower than that of the cluster intermediate. In this case, the rhodium precursor is converted to Rh_{4-6} clusters, and then these clusters agglomerate to form a metal nanoparticle. The rate of reaction, for the conversion of the rhodium clusters into a nanoparticle phase, would be limited by an activation barrier for cluster agglomeration and growth. Another ligand class would include a *strong* ligand in which the free energy of the cluster is lower than that of the nanoparticle phase. In this case the reaction has already proceeded to the minimum energy at the cluster phase and cannot progress to the nanoparticle phase. We briefly explore the hypothesis that the dehydrocoupling reaction involves a *weak* ligand intermediate and that the dehydrocoupling reaction then occurs by the formation of a finite amount of a metal nanoparticle phase. In this case, sufficient metal phase must have formed within 1 h to be coincident with the maximum rate of DMAB dehydrocoupling. Further, the agglomeration process should continue at approximately the *same rate* in the subsequent 72 h after the reaction is initiated. In other words, for this *weak* ligand model, one would expect a nearly 100-fold increase in the metal concentration at this last stage of the reaction. In contrast, the XAFS results show that the rhodium metal concentration is below the detection limit of 1% in this end product (t = 72 h) implying that the rhodium metal concentration during the active DMAB dehydrocoupling (t = 1 h) would be less than 0.01%. It is thus most likely that the amine borane ligands are strong ligands that stabilize the Rh_{4-6} cluster inhibiting agglomeration to a metal nanoparticle.

We have presented a range of XAFS results showing that there is neither metal nor metal nanoparticles present during

(38) Frenkel, A. I.; Hills, C. W.; Nuzzo, R. G. *J. Phys. Chem. B* **2001**, *105*, 12689.

Scheme 1

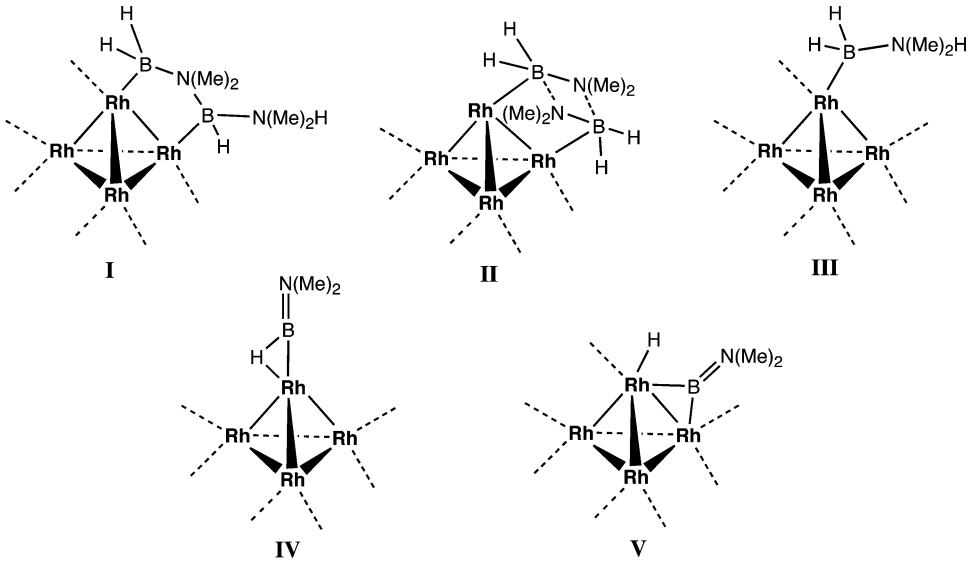

catalysis: (i) the observed rhodium−rhodium distance of 2.73 Å is *longer* than that for rhodium metal (2.68 Å) thus stabilized against agglomeration; (ii) the rhodium−rhodium coordination number is 3.3 which is much smaller than 12 for bulk metal; (iii) there is no evidence of third and fourth rhodium−rhodium shells that exist for nanoparticles or a metal; (iv) there is good sensitivity for a second shell rhodium that is consistent with a small amount of Rh_6 cluster but not nanoparticles; (v) isosbestic points show only two rhodium species, the precursor and the Rh_{4-6} cluster; (vi) the maximum rate of amine borane dehydrocoupling is coincident with the maximum concentrations of Rh_{4-6} clusters (from corresponding NMR kinetic data, not shown); (vii) the precipitate after 72 h under reducing conditions does not contain metal; (viii) added DMAB monomer redissolves the precipitate which is unlikely for rhodium metal; (ix) added DMAB dimer precipitates the active catalyst which is consistent with the cluster model; (x) the induction period observed for the initiation of the dehydrocoupling reaction is consistent with the delay to form the active Rh_{4-6} cluster from the precursor.

In this study we observe 99% of the rhodium containing species present during the reaction. Even though our evidence is extremely strong, we can never rule out the fraction of a percent of the material that may be metallic in nature. However, previous reports stating that the predominant species present during catalysis is metallic rhodium are not consistent with our observations.

4.2. Structure of Ligands on the Rh_{4-6} Catalyst. 4.2.1. From Chloro-(1,5-cyclooctadiene)rhodium (I) Dimer. In previous sections we have shown that the complex contains Rh_{4-6} clusters. Although XAFS has a limited ability to resolve the ligand structure about this cluster, through XAFS studies of related chemical systems it is possible to generate a clear picture of the mostly likely ligand structure. For instance we have previously shown that chloride is not one of the first shell ligands by conducting chemistry on the rhodium cyclooctadiene analogue, bis(1,5-cyclooctadiene)rhodium (I) trifluoromethanesulfonate.

From the $\tilde{\chi}(R)$ plots in Figure 8 we have shown that the amine borane ligands likely bind through the boron atom rather than the nitrogen atoms because the ligand binding region between 1 and 2 Å for a series of primary and secondary amine boranes are all the same. If there was binding through the nitrogen, then the carbon on the alkyl groups in the second shell would weakly contribute to the scattering in the range around 2 Å, which is not observed.

We also modeled a series of different ligand binding geometries according to the structures shown in Scheme 1. Hence in structures **IV** and **V**, we tested the hypothesis that the amine borane would simply replace the CO terminal or bridging sites in $Rh_4(CO)_{12}$ by fitting to the appropriate Rh−B and Rh−N scattering paths generated through FEFF8. In both cases the Rh−N distances were too long with respect to the measured Rh−N distance of 2.67 ± 0.04 Å reported in Table 2. Likewise structure **III**, in which there is a tetrahedral bond about the boron atom, with a Rh−B−N bond angle of approximately 109°, can be discounted on the same basis due to the fact that the Rh−N distance would be too long. On the other hand, both structures **I** and **II** are consistent with the measured distances and coordination numbers for both the Rh−B and Rh−N bonds.

The Rh−N bond distance constrains the Rh−B−N bond angle to slightly less than 90°. This constraint is satisfied by structure **II** involving the cyclic DMAB dimer in a bridging position and by structure **I** involving bridging of the linear dimer. Overall, structure **II** is slightly favored because DiPAB and DCAB do not readily form new intermolecular B−N bonds, and yet the spectra of the observed rhodium complexes for both DMAB and DiPAB/DCAB are nearly identical. The final DCAB or DiPAB products can interact through the pi bonding with another bound R_2NBH_2 product while bound to the rhodium cluster to yield the same type of rhodium−boron and rhodium−nitrogen interactions as the DMAB dimer.

We measure the rhodium−boron distance as 2.095 ± 0.02 Å. Crystallographic data exist for only a few rhodium−boron complexes.[39,40] Organoborane compounds can form rhodium−boron bonds via a dihydridorhodium linkage having a single

(39) Westcott, S. A.; Marder, T. B.; Baker, R. T.; Harlow, R. L.; Calabrese, J. C.; Lam, K. C.; Lin, Z. Y. *Polyhedron* **2004**, *23*, 2665.
(40) Hartwig, J. F.; Cook, K. S.; Hapke, M.; Incarvito, C. D.; Fan, Y. B.; Webster, C. E.; Hall, M. B. *J. Am. Chem. Soc.* **2005**, *127*, 2538.

rhodium−boron bond with a length of 2.17 Å.[39] Dialkoxyboranes (e.g., pinacolborane) can form single rhodium−boron bond having lengths of about 2.07 Å. Dialkoxyboranes also form semibridging rhodium−boron bonds between two rhodium sites with nonequivalent bond lengths of 2.057 and 2.444 Å.[39] Such complexes also include both rhodium−rhodium bridging and rhodium terminal hydride groups. Finally a dirhodium DiPPE complex with B_3H_7 involves one bridging and two terminal rhodium−boron bonds having distances of 2.16 and 2.25 Å, respectively. This species contains both rhodium−rhodium and rhodium−boron bridging hydrides and in addition to a terminal hydride on the rhodium. None of these systems are completely chemically equivalent to the Rh_{4-6} complex that contains Rh−B−N bonds. Overall though the rhodium−boron bond distance for the Rh_{4-6} cluster in this study is most consistent with the rhodium−boron bond distances measured for the dialkoxyborane compounds.

Conclusions

We believe, in contrast to results derived from *ex situ* measurements, we have demonstrated that there is little or no metallic rhodium present during the catalyzed dehydrocoupling of amine boranes. This use of *operando* XAFS sheds light onto a particularly opaque analytical problem. XAFS does not allow the discrimination of absolute structures and does not necessarily yield quantitative information about the number of structures in solution. However in this catalytic system we have shown that the rhodium catalyst precursor compounds cleanly convert to a new set of clusters containing four or six rhodium atoms ligated most likely through the boron atom of the amine borane substrates or amine borane products. All catalyst precursors and all amine borane substrates convert to very similar rhodium clusters. We have shown that the catalytic dehydrocoupling does produce metallic rhodium in the presence of air and that the rhodium clusters can be transformed into metallic rhodium by air oxidation of the borane ligands. Unfortunately one cannot always pin down the exact structure of the active catalyst. In this case the observed rhodium clusters most likely make up a catalyst resting state; however the proposed structures could just as easily be the active catalyst. However unlikely, we cannot rule out that <1% of the unobserved rhodium might be a metallic dehydrocoupling catalyst. In the same way, we cannot rule out a monomeric rhodium complex being the active catalyst. The latter is more amenable to the observed rhodium clusters, especially if the Rh_4 and Rh_6 clusters are in equilibrium with one another (as per eq 6).

We have shown the utility of *operando* XAFS for structural determinations of catalytic, especially homogeneous catalytic, systems. We are currently applying the methods of operando XAFS described herein to help discriminate other homogeneous vs heterogeneous cluster questions.

Acknowledgment. We acknowledge Drs. M. Bullock and D. Dubois for helpful discussions. We also acknowledge the assistance of Alan Willse in the PCA analysis. This work was supported by the U.S. Department of Energy's (DOE) Office of Basic Energy Sciences, Chemical Sciences program. The Pacific Northwest National Laboratory is operated by Battelle for DOE. PNC/XOR facilities at the Advanced Photon Source, and research at these facilities, are supported by the U.S. Department of Energy-Basic Energy Sciences, a major facilities access grant from NSERC, the University of Washington, Simon Fraser University, the Pacific Northwest National Laboratory, and the Advanced Photon Source. Use of the Advanced Photon Source is also supported by the U.S. Department of Energy, Office of Science, Office of Basic Energy Sciences, under Contract DE-AC02-06CH11357.

Supporting Information Available: XAFS spectra and analysis. This material is available free of charge via the Internet at http://pubs.acs.org.

JA073331L